Nanostructures

DOI: 10.1002/ange.201301096

Plasmonic and Catalytic AuPd Nanowheels for the Efficient Conversion of Light into Chemical Energy**

*Xiaoqing Huang, Yongjia Li, Yu Chen, Hailong Zhou, Xiangfeng Duan, and Yu Huang**

Plasmonics is an emerging field of science and technology that exploits the unique optical properties of nanomaterials.[1–4] The plasmonic materials can concentrate light into deep-subwavelength dimensions. This management of photons could be of benefit in a variety of areas, including biomedical imaging/therapy, photovoltaics, solid-state lighting, and display technologies.[5–9] The key components of plasmonic materials are noble metals, since the electromagnetic waves can couple to the collective oscillations of free electrons in the metals.[1,6] The plasmonic features of noble-metal nanostructures are highly dependent on the size, morphology, and composition of the structures. Metal nanocrystals with various structures and compositions have been fabricated by different techniques, such as template-directed fabrication and electrochemical or chemical synthesis.[10–16] Plasmonic nanostructures have mainly been created from Ag/Au-based materials.[1,15] Pd/Pt nanomaterials display little in the way of tunable surface plasmon resonance (SPR) properties as have been widely discovered in Ag/Au nanocrystals.[17,18] The absence of strong SPR absorption has largely inhibited the use of Pd/Pt materials in plasmonics.[19]

Noble metals have an at least equally vital role in the chemical industry as they do in the field of plasmonics. Noble metal nanostructures, especially Pd/Pt-based materials, serve as the primary catalysts for various organic reactions that are invaluable to modern-day life.[20–27] Most commercial catalytic reactions are driven by conventional heating processes. Unfortunately, conventional heating has several negative side effects.[28–31] First, conventional heating processes show essentially low energy efficiencies, because a significant input of thermal energy is needed to run chemical transformations that are inherently exothermic. Second, high operating temperatures compromise the stability and reusability of catalysts. Third, higher operating temperatures decrease the selectivity for the desired products in some partial-oxidation reactions, because the partially oxidized products readily undergo further thermal transformation at high temperatures. The development of new catalytic systems based on new catalysts and a different energy source for effective chemical transformations is highly desirable, but remains a significant challenge.

A merging of the fields of plasmonics and catalysis in noble-metallic nanostructures thus seems natural and extremely beneficial for the creation of new catalyst systems. For the development of such catalyst systems, the construction of novel metal nanostructures that exhibit both unique plasmonic and unique catalytic features is critical. Herein, we report an efficient synthetic strategy that enables the one-pot preparation of novel AuPd nanowheels, a freestanding form of bimetallic AuPd nanostructures that display well-defined but tunable SPR. The synthetic strategy is based on the introduction of the oxidant HNO_3, which can mediate the reduction sequence of $HAuCl_4$ and Na_2PdCl_4. It leads to the formation of unique AuPd nanowheels with only an Au core surrounded by metallic Pd. The average diameter of the nanowheels is synthetically controllable, which leads to tunable SPR properties. More importantly, we show that the AuPd nanowheels can utilize solar energy to drive catalytic reactions, such as the oxidation of benzyl alcohol and Suzuki coupling reactions, at lower temperatures and with much higher performance than possible with the conventional heating processes. These features make the AuPd nanowheels promising for practical and industrial applications.

The bimetallic AuPd nanowheels were prepared by a facile wet-chemical reduction method. In a typical synthesis, aqueous solutions of chloroauric acid ($HAuCl_4$), sodium tetrachloropalladate (Na_2PdCl_4), octadecyltrimethylammonium chloride (OTAC), and nitric acid (HNO_3) were combined in a vial (see the Supporting Information for details). These solutions were mixed to give a homogeneous mixture, and then a freshly prepared aqueous solution of ascorbic acid (AA) was added quickly with stirring. The vial was capped, and the resulting mixture was stirred at room temperature for another 3 h. As the reaction proceeded, the mixture underwent a significant color change from yellow to light yellow, light blue, and finally blue-green. The resulting colloidal products were collected by centrifugation and washed several times with water.

The morphologies of the prepared AuPd nanowheels were initially determined by scanning electron microscopy (SEM), transmission electron microscopy (TEM), and high-angle

[*] X. Huang, Y. Li, Y. Chen, Prof. Y. Huang
Department of Materials Science and Engineering
University of California—Los Angeles
Los Angeles, CA 90095 (USA)
E-mail: yhuang@seas.ucla.edu
H. Zhou, Prof. X. Duan
Department of Chemistry and Biochemistry
University of California—Los Angeles
Los Angeles, CA 90095 (USA)
Prof. X. Duan, Prof. Y. Huang
California Nanosystems Institute
University of California—Los Angeles
Los Angeles, CA 90095 (USA)

[**] We acknowledge the support from ARO, Award 54709-MS-PCS and ONR Award N00014-08-1-0985. We thank EICN at CNSI for the TEM support. Y.H. acknowledges the support of a Sloan Research Fellowship.

Supporting information for this article is available on the WWW under http://dx.doi.org/10.1002/anie.201301096.

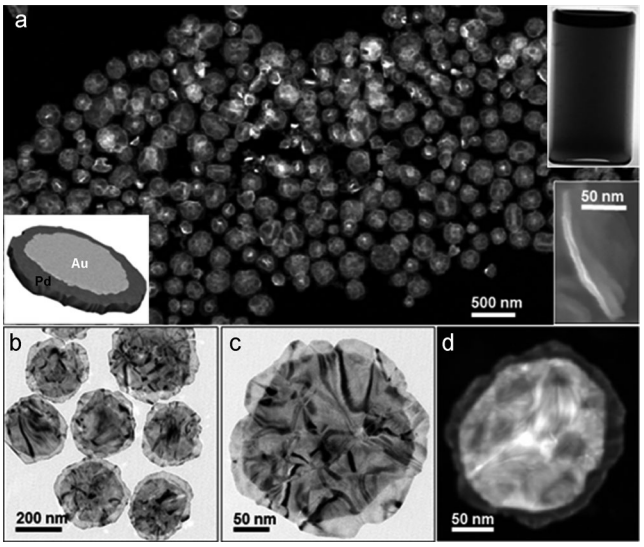

Figure 1. a,b) Representative low-magnification HAADF-STEM (a) and TEM images (b) of the as-prepared AuPd nanowheels. c,d) High-magnification TEM (c) and HAADF-STEM images (d) of an individual AuPd nanowheel. The bottom-right inset in (a) shows an SEM image of an individual AuPd nanowheel viewed from the side. The bottom-left inset in (a) shows an ideal model of a AuPd nanowheel. The top-right inset in (a) shows a photograph of a dispersion of the AuPd nanowheels in water in a glass vial.

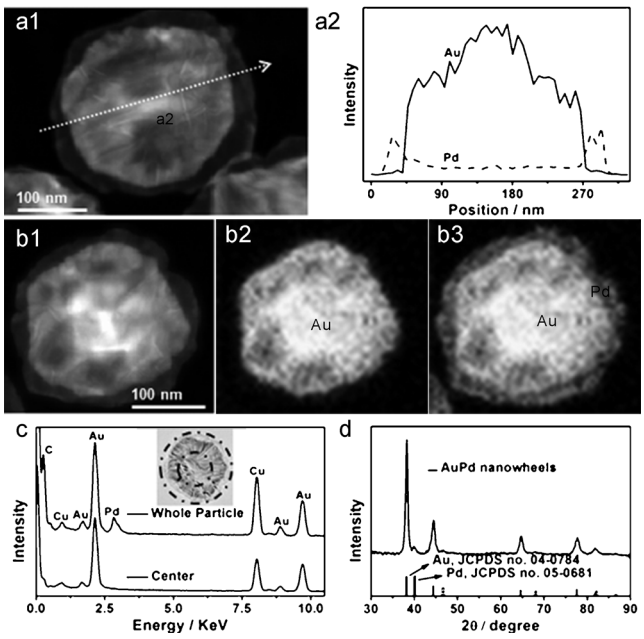

Figure 2. a1,a2) HAADF-STEM image and corresponding EDX line profiles of an individual AuPd nanowheel. b1–b3) HAADF-STEM image and corresponding EDX mapping images of an individual AuPd nanowheel. c) TEM–EDX analysis of the center and whole of a AuPd nanowheel as marked in the inset. d) Powder XRD pattern of the AuPd nanowheels.

annular dark-field scanning TEM (HAADF-STEM; Figure 1), which clearly revealed that the product consisted of platelike structures in a yield approaching 94%. The structures had an average edge length of 290 nm and a thickness of only about 6 nm (inset in Figure 1a). Interestingly, each nanostructure possessed two different regions that contrasted strongly with one another and indicated the possible presence of heterostructures in the nanocrystals. This striking feature is clearly apparent in the high-magnification TEM image (Figure 1c) and HAADF-STEM image (Figure 1d).

To further identify this platelike structure, we used a number of tools to analyze the nanostructures and characterize the element distribution in the nanostructures. Inductively coupled plasma atomic emission spectroscopy revealed that the overall weight percentage of Au in the products was 85.9%, which suggests that the molar ratio of Au to Pd is 76.8:23.2. In the compositional line scanning profiles obtained by HAADF-STEM energy dispersive X-ray spectroscopy (HAADF-STEM-EDX) for an individual nanostructure (Figure 2a), the boundary between the Au and Pd segments can be observed clearly. Elemental mapping of Au and Pd (Figure 2b) also revealed that the nanostructures were composed of different segments. In particular, the as-prepared AuPd nanocrystals are essentially wheel-like nanostructures in which Pd encircles a pure Au core (Figure 2c). We refer to them as AuPd nanowheels herein. The high-resolution TEM (HRTEM) image indicates that both the Au segment and the Pd segment have good crystallization (see Figure S1 in the Supporting Information). The clear fringes in the Au and Pd regions showed periods of 0.24 and 0.22 nm, respectively, as expected for face-centered cubic (fcc) Au(111) and Pd(111) planes. The powder X-ray diffraction (XRD) pattern of the products (Figure 2d) showed two distinct sets of diffraction peaks, which were assigned to the fcc structure of Au and Pd and which indicated that no alloyed phase existed in the products. Thus, all the data fully confirm the successful creation of bimetallic AuPd nanowheels.

The ability to prepare bimetallic AuPd nanowheels in one pot is the most striking feature of this synthesis. Bimetallic AuPd nanowheels of this kind have not been synthesized previously. To better understand the growth process of the AuPd nanowheels in our system, we monitored their growth under the typical synthetic conditions. The growth intermediates of the AuPd nanowheels were collected at different reaction times. TEM and EDX analysis showed that only polycrystalline Au nanostructures had been formed after 1 min (Figure 3). We believe that the roughness of the nanowheels has its origin in the polycrystalline nature of the preformed Au nanostructures. When the reaction time was increased to 2 min, many small nanoparticles were found around the preformed Au nanostructures (Figure 3b). HAADF-STEM mapping confirmed that these newly formed nanoparticles were composed of Pd (Figure 3c). The Pd nanoparticles aggregated around the preformed Au nanocrystals (Figure 3d). The portion of Pd was around 3% at this time. Within just 20 min (Figure 3e), a nearly continuous ring of Pd formed around the Au core. Thus, the growth process of the Pd ring follows the Ostwald ripening mechanism.[31] Together with the appearance of the wheel-like structure, an increase in the Pd content of the nanostructures was evidenced after a reaction time of 60 min (Figure 3f). When the reaction time was increased further to 180 min, the wheel-

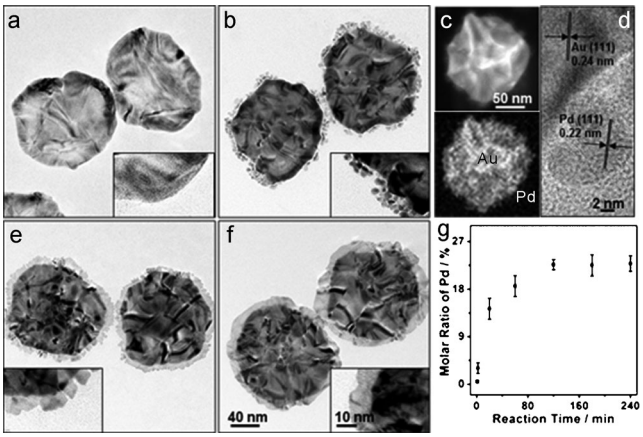

Figure 3. a,b,c,d) TEM images of growth intermediates of AuPd nanowheels produced in reactions carried out for 1 min (a), 2 min (b), 20 min (c), and 60 min (d). Scale bars in (d) apply to all images (the 40 nm scale bar for the main image, the 10 nm scale bar for the inset). e) HAADF-STEM image, EDX mapping image, and f) HRTEM image at the boundary of an intermediate of an AuPd nanowheel produced in a reaction carried out for 2 min. g) Change in the molar ratio of Pd in the nanostructures during the reaction, as determined by TEM–EDX analysis.

like structure became more distinct (Figure 1). The Pd/Au ratio in the sample after 180 min was close to the ratio supplied in the reactions. Beyond 180 min, up to a reaction time of 240 min, no significant change in the structure was observed (Figure 3 g). Therefore, it can be concluded that the formation of bimetallic AuPd nanowheels relies upon the initial formation of Au nanostructures and the subsequent growth of Pd around the edge of the preformed Au nanostructures through an Ostwald ripening mechanism.

To further understand the growth mechanism involved in the formation of the AuPd nanowheels, the reagents used for their synthesis were investigated in detail in a set of control experiments. In the synthesis, the use of HNO_3 was critical for the formation of AuPd nanowheels. When HNO_3 was left out of the reaction mixture or replaced with HCl or H_2SO_4, the reaction did not yield AuPd nanowheels (see Figure S3 in the Supporting Information). We also observed that the reaction without HNO_3 gave a colloidal solution within 5 s, whereas the reaction mixture containing HNO_3 appeared unchanged after 5 s, and no separable particles were obtained until a reaction time of 40 s had elapsed. This phenomenon indicates that HNO_3 retards the apparent reduction of metal precursors. It is reasonable to believe that the reduction is retarded as a result of the oxidative etching effect induced by HNO_3, which is a well-known oxidant and can dissolve the reduced metal atoms.[32] Furthermore, the difference in the reduction kinetics of Au and Pd precursors in our system is probably associated with the fact that Pd is more reactive and more susceptible to oxidation than Au ($AuCl_4^-$/Au, +1.002 V versus SHE (standard hydrogen electrode); $PdCl_4^{2-}$/Pd, +0.591 V versus SHE).[33]

On the basis of the above growth mechanism, it is expected that the growth of AuPd nanowheels should be greatly affected by the amount of HNO_3 present. This expectation was indeed confirmed experimentally. When the other reaction conditions were maintained unchanged and the amount of aqueous HNO_3 (1.0 M) was increased from 2.0 to 3.0 and then 4.0 mL, the size of the AuPd nanowheels increased from 290 to 450 and 750 nm (see Figure S4). Thus, when more of the oxidant (HNO_3) is present in the reaction mixture, less nucleus is formed during the early stage of the reaction, and as a result, larger AuPd nanowheels are formed. We also found that the use of OTAC is important for the synthesis of nanowheels with good dispersity and a well-defined shape. Reactions in the absence of OTAC or with a smaller amount of OTAC (0.10 rather than 0.35 mL) under otherwise unchanged experimental conditions led to the formation of heavily aggregated particles (see Figure S5 a–d). Although AuPd nanowheels were still obtained when OTAC was replaced with cetyltrimethylammonium chloride (CTAC; see Figure S5 e,f), reactions in the presence of octadecyltrimethylammonium bromide (OTAB) instead of OTAC did not yield AuPd nanowheels (see Figure S5 g,h). This result indicates that the Cl^- ion in OTAC also plays an important role in the growth of AuPd nanowheels.[34]

One striking feature of the obtained nanowheels is that they exhibit well-defined SPR properties (Figure 1 a, inset). Motivated by the fact that the SPR properties of metal nanostructures are typically dependent on size and composition, we developed strategies to control the size and composition of the AuPd nanowheels. First, by simply controlling the molar ratios of the Au and Pd precursors supplied in the reaction, we readily obtained AuPd nanowheels with a controlled Au/Pd content by the same synthetic procedure. An increase in the amount of aqueous Na_2PdCl_4 (10 mM) supplied from 0.12 to 0.24 and 0.36 mL led to an increase in the average size of the Pd edge in the AuPd nanowheels from 37 to 62 and 85 nm (see Figure S6 a–c). Together with the increased size of the Pd domains, the size of the nanowheels also increased from 290 to 390 and 502 nm. The average diameter of the AuPd nanowheels could be controlled by varying the amount of ascorbic acid (AA). When the other reaction conditions were maintained unchanged, AuPd nanowheels grown with 0.2, 0.4, and 1.0 mL of aqueous AA (0.1 M) had an average size of 620, 390, and 180 nm, respectively (see Figure S6 d–f). Accordingly, the SPR peak of the AuPd nanowheels was blue-shifted from 1176 to 992 and 846 nm when the edge length was reduced from 620 to 390 and 180 nm, respectively (see Figure S7).

The unique heterostructure and optical properties of the as-prepared bimetallic AuPd nanowheels offer the possibility of light-enhanced catalytic applications. We chose two heterogeneous catalytic reactions (the oxidation of benzyl alcohol and a Suzuki coupling reaction) to evaluate the catalytic activity of the nanowheels under irradiation with light.[35–38] For the studies on the oxidation of benzyl alcohol, AuPd nanowheels, *tert*-butyl hydroperoxide (TBHP), and an ethanol/water mixture were used as the catalyst, oxidant, and solvent, respectively. The reaction mixtures were immerged in an oil bath set at 50 °C and exposed to irradiation with a xenon lamp (power density ca. 0.37 W cm^{-2}) under vigorous stirring. We also conducted a similar catalytic reaction, but without

irradiation with light, for comparison (i.e. under conventional heating conditions). The reaction temperature for the two processes (light irradiation and conventional heating) was controlled by the oil bath and kept constant. To demonstrate the structural advantage of the AuPd nanowheels, we also used single-component Au nanostructures and Pd nanostructures as well as a mixture of Au and Pd nanostructures for comparison; these single-component nanostructures were prepared under similar synthetic conditions to those used for the synthesis of the nanowheels (see Figure S8).

In Figure 4a, the formation of the reaction product is plotted against time for the oxidation of benzyl alcohol with and without light irradiation. We can see that under irradiation with light, the oxidation reaction proceeds very fast: nearly 97.7% conversion of benzyl alcohol into benzaldehyde occurred with almost 98.0% selectivity within 6 h. However, with conventional heating under otherwise identical experimental conditions, only 18.4% of the benzyl alcohol was converted into benzaldehyde in 6 h. When the AuPd nanowheels were replaced with Au nanostructures, Pd nanostructures, or a mixture of Au and Pd nanostructures, we also did not observe the efficient conversion of benzyl alcohol (see Table S1 in the Supporting Information). We infer that the enhanced activity may be attributed to the interface interaction between Au and Pd segments in the nanowheel.[39,40] Similar behavior was also found in the Suzuki coupling reaction (Figure 4b; see also Table S2), for which AuPd nanowheels under irradiation with light showed the best activity: 3.8 times greater than that observed under conventional heating conditions (on the basis of the conversion at 60 min). These results clearly show that the unique structure of the AuPd nanowheels significantly enhanced not only their catalytic activity but also their ability to exploit the light. This ability was vital to the development of a new catalyst system that could effectively drive chemical conversion under mild conditions.

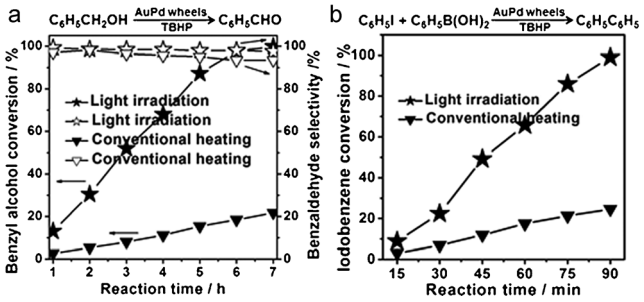

Figure 4. a) The conversion of benzyl alcohol as a function of time (left axis, filled symbols) and selectivity for the formation of benzaldehyde (right axis, open symbols) during the oxidation of benzyl alcohol and b) the conversion of iodobenzene as a function of time during the Suzuki coupling reaction under irradiation with light or conventional heating conditions. The power density is 0.37 Wcm^{-2}. The temperature is 50°C.

ature and light intensity. In reactions to determine the reaction-temperature dependence, an oil bath was used to modulate the temperature of the reaction. Figure 5a shows the measured conversions in the conventional heating process (no light) and under irradiation with light as a function of operating temperature. It also shows the conversion enhancement, calculated as the conversion under irradiation with light divided by the conversion under conventional heating, as a function of temperature. The conversion enhancement decreased as a function of temperature from about 9.0-fold at lower temperatures to about 2.3-fold at higher temperatures. In the reactions to determine the light-intensity dependence, a photometer was used to modulate the intensity of the light. Each experiment was carried out three times to ensure consistency. Figure 5b shows the enhancement factor due to irradiation with light rather than conventional heating for the AuPd nanowheels as a function of the light intensity. The results clearly show a linear dependence of the light-irradiation enhancement factor on the irradiation intensity and thus demonstrate that the plasmon resonance of the metal nanowheels is the primary factor responsible for the light-enhanced activity of the AuPd nanowheels. Parallel studies on Suzuki coupling under irradiation with light gave qualitatively similar results (Figure 5c,d) and further confirmed the strong plasmonic enhancement of the activity of the AuPd nanowheels. Overall, these results show that the interaction of AuPd nanowheel catalysts with light led to

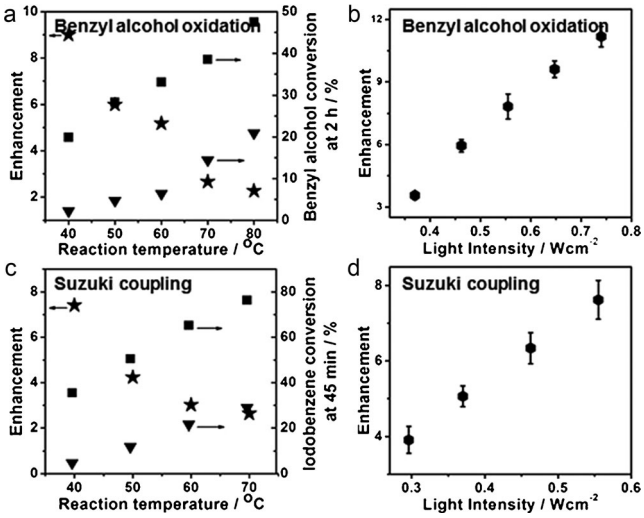

Figure 5. a,c) Rate enhancement (left axis, stars) as calculated by dividing the conversion of the light-irradiation process by the conversion of the conventional heating process as a function of temperature for the benzyl alcohol oxidation (a) and Suzuki coupling reaction (c). The right axis shows the conversions of the conventional heating process (triangles) and the light-irradiation method (squares) as a function of temperature. The power density is 0.37 Wcm^{-2}. b,d) Rate enhancement calculated by dividing the conversion of the light-irradiation process by the conversion of the conventional heating process as a function of light intensity for the benzyl alcohol oxidation (b) and Suzuki coupling reaction (d). The temperature is 50°C.

a significant increase in the conversions of the catalytic reactions.

In summary, we have developed an efficient one-pot strategy for the production of bimetallic AuPd nanowheels with a controllable edge length and tunable SPR features. These unique bimetallic nanowheels can be used as a platform for studying the physicochemical properties of heterostructured nanomaterials and will find a number of optical and catalytic applications. For example, the prepared AuPd nanowheels served as highly efficient catalysts in the oxidation of benzyl alcohol and a Suzuki coupling reaction under irradiation with light. Much enhanced performance was observed relative to that under conventional heating conditions. The light-enhanced catalytic performance could be attributed to the unique heterostructure and SPR of the AuPd nanowheels. Given the distinct chemical nature of Au and Pd in the AuPd nanowheels, together with the property of SPR, superior catalytic and analytical systems can be developed with these nanowheels.

Received: February 6, 2013
Published online: April 24, 2013

Keywords: gold · heterogeneous catalysis · nanowheels · palladium · plasmonics

[1] M. Rycenga, C. M. Cobley, J. Zeng, W. Y. Li, C. H. Moran, Q. Zhang, D. Qin, Y. N. Xia, *Chem. Rev.* **2011**, *111*, 3669 – 3712.
[2] M. R. Jones, K. D. Osberg, R. J. Macfarlane, M. R. Langille, C. A. Mirkin, *Chem. Rev.* **2011**, *111*, 3736 – 3827.
[3] S. Linic, P. Christopher, D. B. Ingram, *Nat. Mater.* **2011**, *10*, 911 – 921.
[4] J. A. Schuller, E. S. Barnard, W. S. Cai, Y. C. Jun, J. S. White, M. L. Brongersma, *Nat. Mater.* **2010**, *9*, 193 – 204.
[5] M. E. Stewart, C. R. Anderton, L. B. Thompson, J. Maria, S. K. Gray, J. A. Rogers, R. G. Nuzzo, *Chem. Rev.* **2008**, *108*, 494 – 521.
[6] P. K. Jain, X. H. Huang, I. H. El-Sayed, M. A. El-Sayed, *Acc. Chem. Res.* **2008**, *41*, 1578 – 1586.
[7] N. Calander, *Curr. Anal. Chem.* **2006**, *2*, 203 – 211.
[8] J. R. Krenn, *Nat. Mater.* **2003**, *2*, 210 – 211.
[9] E. M. Larsson, C. Langhammer, I. Zoric, B. Kasemo, *Science* **2009**, *326*, 1091 – 1094.
[10] P. K. Jain, X. Huang, I. H. El-Sayed, M. A. El-Sayad, *Plasmonics* **2007**, *2*, 107 – 118.
[11] C. J. Murphy, T. K. San, A. M. Gole, C. J. Orendorff, J. X. Gao, L. Gou, S. E. Hunyadi, T. Li, *J. Phys. Chem. B* **2005**, *109*, 13857 – 13870.
[12] R. C. Jin, Y. C. Cao, E. C. Hao, G. S. Métraux, G. C. Schatz, C. A. Mirkin, *Nature* **2003**, *425*, 487 – 490.
[13] R. C. Jin, Y. W. Cao, C. A. Mirkin, K. L. Kelly, G. C. Schatz, J. G. Zheng, *Science* **2001**, *294*, 1901 – 1903.
[14] X. H. Huang, S. Neretina, M. A. El-Sayed, *Adv. Mater.* **2009**, *21*, 4880 – 4910.
[15] M. Hu, J. Y. Chen, Z.-Y. Li, L. Au, G. V. Hartland, X. D. Li, M. Marquez, Y. N. Xia, *Chem. Soc. Rev.* **2006**, *35*, 1084 – 1094.
[16] X. Huang, S. Li, Y. Huang, S. Wu, X. Zhou, S. Li, C. Gan, F. Boey, C. A. Mirkin, H. Zhang, *Nat. Commun.* **2011**, *2*, 292 – 297.
[17] Y. N. Xia, Y. J. Xiong, B. Lim, S. E. Skrabalak, *Angew. Chem.* **2009**, *121*, 62 – 108; *Angew. Chem. Int. Ed.* **2009**, *48*, 60 – 103.
[18] N. J. Halas, *Nano Lett.* **2010**, *10*, 3816 – 3822.
[19] C. Langhammer, Z. Yuan, I. Zorić, B. Kasemo, *Nano. Lett.* **2006**, *6*, 833 – 838.
[20] A. C. Chen, P. Holt-Hindle, *Chem. Rev.* **2010**, *110*, 3767 – 3804.
[21] Z. M. Peng, H. Yang, *Nano Today* **2009**, *4*, 143 – 164.
[22] F. Favier, E. C. Walter, M. P. Zach, T. Benter, R. M. Penner, *Science* **2001**, *293*, 2227 – 2231.
[23] Y. J. Xiong, Y. N. Xia, *Adv. Mater.* **2007**, *19*, 3385 – 3391.
[24] X. Q. Huang, S. H. Tang, X. L. Mu, Y. Dai, G. X. Chen, Z. Y. Zhou, F. X. Ruan, Z. L. Yang, N. F. Zheng, *Nat. Nanotechnol.* **2011**, *6*, 28 – 32.
[25] C. Y. Chiu, Y. J. Li, L. Y. Ruan, X. C. Ye, C. B. Murray, Y. Huang, *Nat. Chem.* **2011**, *3*, 393 – 399.
[26] C. H. Kuo, Y. Tang, L. Y. Chou, B. T. Sneed, C. N. Brodsky, Z. P. Zhao, C. K. Tsung, *J. Am. Chem. Soc.* **2012**, *134*, 14345 – 14348.
[27] D. S. Wang, Y. D. Li, *Adv. Mater.* **2011**, *23*, 1044 – 1060.
[28] C. T. Campbell, S. C. Parker, D. E. Starr, *Science* **2002**, *298*, 811 – 814.
[29] Y. Lei, F. Mehmood, S. Lee, J. Greeley, B. Lee, S. Seifert, R. E. Winans, J. W. Elam, R. J. Meyer, P. C. Redfern, D. Teschner, R. Schlögl, M. J. Pellin, L. A. Curtiss, S. Vajda, *Science* **2010**, *328*, 224 – 228.
[30] A. Wittstock, V. Zielasek, J. Biener, C. M. Friend, M. Baumer, *Science* **2010**, *327*, 319 – 322.
[31] C. L. Lu, K. S. Prasad, H. L. Wu, J. A. A. Ho, M. H. Huang, *J. Am. Chem. Soc.* **2010**, *132*, 14546 – 14553.
[32] R. Laocharoensuk, S. Sattayasamitsathit, J. Burdick, P. Kanatharana, P. Thavarungkul, J. Wang, *ACS Nano* **2007**, *1*, 403 – 408.
[33] Y. W. Lee, M. Kim, Z. H. Kim, S. W. Han, *J. Am. Chem. Soc.* **2009**, *131*, 17036 – 17037.
[34] Y. Ma, Q. Kuang, Z. Jiang, Z. Xie, R. Huang, L. Zheng, *Angew. Chem.* **2008**, *120*, 9033 – 9036; *Angew. Chem. Int. Ed.* **2008**, *47*, 8901 – 8903.
[35] F. Wang, C. H. Li, L. D. Sun, H. S. Wu, T. A. Ming, J. F. Wang, J. C. Yu, C. H. Yan, *J. Am. Chem. Soc.* **2011**, *133*, 1106 – 1111.
[36] R. A. Sheldon, I. W. C. E. Arends, G. J. Ten Brink, A. Dijksman, *Acc. Chem. Res.* **2002**, *35*, 774 – 781.
[37] S. W. Kim, M. Kim, W. Y. Lee, T. Hyeon, *J. Am. Chem. Soc.* **2002**, *124*, 7642 – 7643.
[38] J. Fan, Y. H. Dai, Y. L. Li, N. F. Zheng, J. F. Guo, X. Q. Yan, G. D. Stucky, *J. Am. Chem. Soc.* **2009**, *131*, 15568 – 15569.
[39] X. Huang, Y. Li, H. Zhou, X. Zhong, X. Duan, Y. Huang, *Chem. Eur. J.* **2012**, *18*, 9505 – 9510.
[40] C. Wang, C. J. Xu, H. Zeng, S. H. Sun, *Adv. Mater.* **2009**, *21*, 3045 – 3052.

